Journal of Zhejiang University-SCIENCE A (Applied Physics & Engineering)
ISSN 1673-565X (Print); ISSN 1862-1775 (Online)
www.zju.edu.cn/jzus; www.springerlink.com
E-mail: jzus@zju.edu.cn

A semi-analytical method and its application for calculating the thermal stress and displacement of sparsely fractured rocks with water flow and heat transfer*

Yong ZHANG[1,2], Yan-yong XIANG[†‡1]

([1]*School of Civil Engineering, Beijing Jiaotong University, Beijing 100044, China*)

([2]*Shenhua Group Co. Ltd., Science and Technology Development Division, Beijing 100011, China*)

[†]E-mail: xiang_yanyong@263.net

Received Dec. 21, 2014; Revision accepted July 17, 2015; Crosschecked Oct. 12, 2015

Abstract: Using Goodier's thermo-elastic displacement potential and Laplace transform, a semi-analytical method is developed for calculating the displacement and stress induced by heat transfer in sparsely fractured granitic rocks with saturated water flow and distributed heat sources. An integral equation of the thermo-elastic displacement potential is formulated in the Laplace-transformed domain. The fractures are discretized into rectangular elements, and the elemental integrals that involve singularities are calculated analytically. The numerical solutions of the potential are calculated using numerical Laplace inversion, and the temperature-gradient-induced displacements and stresses are calculated using central differences. The method is employed to examine the characteristics of the temperature-gradient-induced displacement and stress for a hypothetical problem that is intended to mimic the near-field environment of deep geological repositories of high-level radioactive wastes. Among other things, the results reveal the following: (1) In early time of operation of the repository, the region of rock under thermal expansion and compressive is limited; (2) As the intensity of the heat source gets smaller with time, only a small portion of the rock expands whereas the remaining portion contracts; (3) Downstream peak temperatures may be higher due to the supply of thermal energy by the water-flow-facilitated heat transfer, and patterns of influences of the water velocities on the thermal stress and displacement are similar; (4) Sufficiently close heat sources would cause superposition of the heating effects and make the near-field temperature increase significantly.

Key words: Sparsely fractured rock, Water flow, Heat transfer, Thermo-elastic displacement potential, Thermal stress
doi:10.1631/jzus.A1400364 **Document code:** A **CLC number:** TU452

1 Introduction

In the near field of a deep geological repository of high-level nuclear waste, the heat generated by the decay of radionuclides would cause rise in temperatures, thermal stress, and displacement in the host rocks and hence affect its hydrological, mechanical, and chemical properties as well as the repository's capabilities in confining, retarding, and diluting the radioactive nuclides for protection of the far-field environment. Therefore, heat transfer and, in particular, the accompanying thermal stress and displacement effects in the host rock should be analyzed in repository design and performance assessment.

Tortike and Ali (1991; 1993) used the finite element method to solve a hydro-thermo-mechanical coupling model for thermal extraction of petroleum, and determined the distributions of temperature,

‡ Corresponding author

* Project supported by the National Natural Science Foundation of China (No. 51378055), the Research Fund for the Doctoral Program of Higher Education of China (No. 20120009110022), and the National Key Technology Research and Development Program of the Ministry of Science and Technology of China (No. 2013 BAB10B06)

ORCID: Yong ZHANG, http://orcid.org/0000-0003-3248-5463

water saturation, and stress in oil sands. Onofrei and Gray (1996) studied the feasibility of mudstone to host nuclear waste via both physical model test and numerical simulation of coupled hydro-thermo-mechanical processes. Gutierrez and Makurat (1997) numerically analyzed the coupled hydro-thermo-mechanical processes involved in the injection of cold water into a petroleum reservoir in fractured rocks and its effect on the fracture structures and the efficiency of petroleum extraction. Rutqvist *et al.* (2001) conducted a heater test in a mine drift in fractured rock and numerically analyzed the relevant hydro-thermo-mechanical process. Ghassemi and Zhang (2006) analyzed the influence of water pressure and thermal stress on the fracture aperture by using a displacement discontinuity method. Zhou *et al.* (2009) developed a method for the calculation of water pressure and thermal stress in a rock containing one single fracture and analyzed the effects of water injection-extraction on the fracture aperture during geothermal exploration.

This paper presents a semi-analytical method for calculating the displacement and stress induced by heat transfer in sparsely fractured granitic rocks with saturated water flow and distributed heat sources, in an attempt to examine the characteristics of the temperature-gradient-induced displacement and stress for a hypothetical near-field environment of deep geological repositories of high-level radioactive wastes.

2 Temperature equations and its semi-analytical solution

Fig. 1 shows an infinite 3D model of saturated, sparsely fractured rocks with a homogeneous and impermeable matrix (Zhang and Xiang, 2014). Let Ω be the rock matrix domain, T_0 the uniform initial temperature, A_k the surface area, and $\boldsymbol{n}_k$ the unit normal vector of the planes of discrete fractures k=1–K of arbitrary shapes, with K the total number of fractures effective for the heat transfer process. Let p_r be the linear intensity of the heat source distributed along the line Γ, and ρ_r, c_r, and λ_r be the density, specific heat, and thermal conductivity of the rock, respectively. Let ρ_w, c_w, and $\boldsymbol{q}_k$ be the density, specific heat, and prescribed steady unit-width flux (vector) of water in fractures k=1–K, respectively.

Assuming small fracture apertures and instantaneous thermodynamic equilibrium at the fracture walls between the rock matrix and water in the fractures, and negligible thermal diffusion, dispersion, and storage in water in the fractures, the equation for the conservation of thermal energy of water in fractures k=1–K can be expressed as

$$\rho_\mathrm{w} c_\mathrm{w} \boldsymbol{q}_k(x,y,z)\cdot\nabla_3 T(x,y,z,t) - 2\lambda_\mathrm{r}\frac{\partial T(x,y,z,t)}{\partial \boldsymbol{n}_k} = 0,\quad (x,y,z)\in A_k. \tag{1}$$

For the 3D heat conduction in the impermeable rock matrix, the governing equation can be written as

$$\lambda_\mathrm{r}\nabla_3^2 T(x,y,z,t) = \rho_\mathrm{r} c_\mathrm{r}\frac{\partial T(x,y,z,t)}{\partial t} - p'_\mathrm{r}\delta(x-x_p,y-y_p,z-z_p),\ (x,y,z)\in\Omega, \tag{2}$$

where $T(x, y, z, t)$ is the temperature of the point (x, y, z) at time t, ∇_3^2 is the 3D Laplace operator, ∇_3 is the 3D Hamilton operator, $\delta(x–x_p, y–y_p, z–z_p)$ is the 3D Dirac function with (x_p, y_p, z_p) as source point, p'_r is the intensity of a point heat source in the rock matrix, $p_\mathrm{r}=p'_\mathrm{r}\delta(\gamma–\gamma_p)$, with p_r being the intensity of linear heat source, γ and γ_p the line coordinates along Γ.

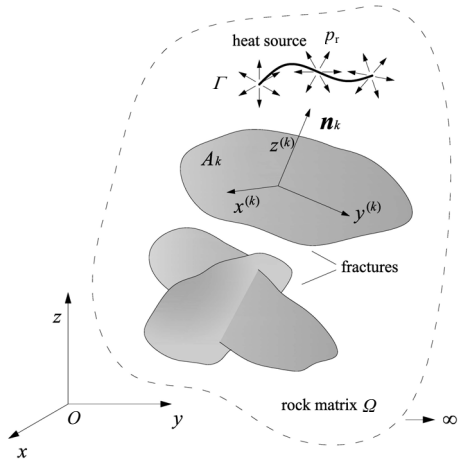

Fig. 1 3D conceptual model for calculations of temperature and thermal stress in sparsely fractured rocks. Reprinted from (Zhang and Xiang, 2014), Copyright 2014, with permission from Elsevier

The boundary and initial conditions for Eqs. (1) and (2) are

$$T(x\to\pm\infty,y,z,t)=T_0, \tag{3a}$$

$$T(x,y\to\pm\infty,z,t)=T_0, \tag{3b}$$

$$T(x,y,z\to\pm\infty,t)=T_0, \tag{3c}$$

$$T(x,y,z,t=0)=T_0,\ (x,y,z)\in\Omega. \tag{3d}$$

A semi-analytical method, as described in Zhang and Xiang (2014), can be employed to determine the spatial distribution and temporal evolution of the temperature of the rock matrix and the fracture water.

3 Thermal elastic equations and its semi-analytical solution

Assume that the influences of the temperature variations on the physical and mechanical properties of the rock matrix and both the deformation and its rate are small and can be neglected. Let α_r, μ, and ν be the thermal expansion coefficient, the shear modulus, and Poisson's ratio of the rock matrix, respectively; ignoring the body force, then the thermal elastic equation for the rock matrix can be written in tensor form as (Wang, 1989)

$$\nabla_3^2 u_i+\frac{1}{1-2\nu}\frac{\partial e}{\partial x_i}=2\alpha_r\frac{1+\nu}{1-2\nu}\frac{\partial T}{\partial x_i},\quad i=1,2,3, \tag{4}$$

where u_i denotes the temperature-gradient-induced displacement in the x_i direction, ∇_3^2 is the Laplace operator in three dimensions, and e and T are the volumetric strain and the transient temperature of the rock matrix, respectively.

The solution of Eq. (4) can be expressed as

$$u_i=u_i^T+u_i^M, \tag{5}$$

where u_i^T denotes the particular solution that represents the temperature-gradient-induced displacement in the x_i direction, and u_i^M is the general solution of the corresponding homogeneous counterpart of Eq. (4) that represents the displacement in the x_i direction to supplement u_i^T so that the total displacement u_i can satisfy the boundary conditions of Eq. (4). Zhang and Xiang (2015) have developed a semi-analytical method of calculating the supplementary (constraint-induced) displacement u_i^M and the total displacement u_i for a rock mass with a single fracture, whereas here we focus only on the temperature-gradient-induced displacement u_i^T.

Let $\Phi=\Phi(x_1, x_2, x_3, T, t)$ be the thermal elastic potential such that

$$u_i^T=\partial\Phi/\partial x_i. \tag{6}$$

Substituting Eq. (6) into Eq. (4), integrating, and letting the integral function of T and t to be zero, we arrive at the governing equation in terms of Φ:

$$\frac{\partial(\nabla_3^2\Phi)}{\partial x_i}=\alpha_r\frac{1+\nu}{1-\nu}\frac{\partial T}{\partial x_i}. \tag{7}$$

The corresponding thermal stress can be calculated using the constitutive equation of elasticity,

$$\sigma_{ij}^T=2\mu\left(\frac{\partial^2\Phi}{\partial x_i\partial x_j}-\delta_{ij}\frac{\partial^2\Phi}{\partial x_k\partial x_k}\right), \tag{8}$$

where δ_{ij} is the Kronecker delta.

According to Carslaw and Jaeger (1959), the temperature increment of the point (x, y, z) at time t induced by a heat source of unit flux intensity of point (x', y', z') at time t' is

$$T^*(x,y,z,x',y',z',t-t')=\sqrt{\frac{\rho_r c_r}{\left[4\pi\lambda_r(t-t')\right]^3}}\exp\left[-\frac{\rho_r c_r R^2}{4\lambda_r(t-t')}\right]. \tag{9}$$

Correspondingly, the thermal elastic potential is

$$\Phi^*(x,y,z,x',y',z',t-t')=-\frac{\alpha_r(1+\nu)}{4\pi\rho_r c_r(1-\nu)R}\operatorname{erf}\left[\frac{R}{2}\sqrt{\frac{\rho_r c_r}{\lambda_r(t-t')}}\right], \tag{10}$$

where $R=\sqrt{(x'-x)^2+(y'-y)^2+(z'-z)^2}$.

For the model shown in Fig. 1, the temperature increment and the thermal elastic potential are due to the combined effects of both the distributed heat source and the heat exchange between the rock matrix and the fracture water. Let $p_f^k(x',y',z',t')$ be the (area) heat flux intensity of the rock matrix and

fracture water heat exchange at point (x', y', z') of fracture k at time t', and let $p_r(x', y', z', t')$ be the (line) heat flux intensity at point (x', y', z') of the linear heat source at time t'. Then the resultant thermal elastic potential at time t can be expressed as

$$\begin{aligned}&\Phi(x,y,z,t)\\&=\sum_{i=1}^{K}\int_0^t\int_{A_k} p_f^k(x',y',z',t')\Phi^*(x,y,z,x',y',z',t-t')\mathrm{d}A_k\mathrm{d}t'\\&+\int_0^t\int_{\Gamma} p_r(x',y',z',t')\Phi^*(x,y,z,x',y',z',t-t')\mathrm{d}\Gamma\mathrm{d}t'.\end{aligned}\tag{11}$$

Taking the Laplace transform of Eq. (11) and using the convolution theorem

$$\mathscr{L}\left[\int_0^t f_1(t)f_2(t-\tau)\mathrm{d}\tau\right]=\tilde{f}_1(s)\tilde{f}_2(s),\tag{12}$$

and we obtain:

$$\begin{aligned}&\tilde{\Phi}(x,y,z,s)=\mathrm{L}\left[\Phi(x,y,z,t)\right]\\&=\sum_{i=1}^{K}\int_{A_k}\tilde{p}_f^k\left(x',y',z',s\right)\tilde{\Phi}^*(x,y,z,x',y',z',s)\mathrm{d}A_k\\&+\int_{\Gamma}\tilde{p}_r\left(x',y',z',s\right)\tilde{\Phi}^*(x,y,z,x',y',z',s)\mathrm{d}\Gamma,\end{aligned}\tag{13}$$

where $\mathscr{L}[\ ]$ denotes the Laplace transform, s is the Laplace parameter, $\tilde{f}_1(s)=\mathscr{L}[f_1(t)]$, $\tilde{f}_2(s)=\mathscr{L}[f_2(t)]$,

$$\begin{aligned}&\tilde{\Phi}^*(x,y,z,x',y',z',s)=\mathscr{L}\left[\Phi^*(x,y,z,x',y',z',t)\right]\\&=\frac{-\alpha_r(1+\nu)}{4\pi s\rho_r c_r(1-\nu)R}\left[1-\exp\left(-\sqrt{\frac{s\rho_r c_r}{\lambda_r}}R\right)\right].\end{aligned}\tag{14}$$

As in Zhang and Xiang (2014) (Fig. 2), for fracture k =1–K, the transformation from the global $oxyz$ system to the local $o^{(k)}x^{(k)}y^{(k)}z^{(k)}$ system can be written as

$$(x^{(k)},y^{(k)},z^{(k)},1)=(x,y,z,1)\boldsymbol{C}^{(k)}\boldsymbol{F}^{(k)},\tag{15}$$

where

$$\boldsymbol{C}^{(k)}=\begin{bmatrix}1&0&0&0\\0&1&0&0\\0&0&1&0\\-x_0^{(k)}&-y_0^{(k)}&-z_0^{(k)}&1\end{bmatrix}$$

is the translation matrix,

$$\boldsymbol{F}^{(k)}=\begin{bmatrix}u_{x^{(k)}x}&u_{y^{(k)}x}&u_{z^{(k)}x}&0\\u_{x^{(k)}y}&u_{y^{(k)}y}&u_{z^{(k)}y}&0\\u_{x^{(k)}z}&u_{y^{(k)}z}&u_{z^{(k)}z}&0\\0&0&0&1\end{bmatrix}$$

is the rotation matrix, $(x_0^{(k)}, y_0^{(k)}, z_0^{(k)})$ are the coordinates of the origin of the local $o^{(k)}x^{(k)}y^{(k)}z^{(k)}$ system, and

$$\begin{cases}\boldsymbol{u}_x^{(k)}=(u_{x^{(k)}x},u_{x^{(k)}y},u_{x^{(k)}z})\\\boldsymbol{u}_y^{(k)}=(u_{y^{(k)}x},u_{y^{(k)}y},u_{y^{(k)}z})\\\boldsymbol{u}_z^{(k)}=(u_{z^{(k)}x},u_{z^{(k)}y},u_{z^{(k)}z})\end{cases}$$

are the directional unit vectors of the local $o^{(k)}x^{(k)}y^{(k)}z^{(k)}$ coordinates with respect to the global $oxyz$ coordinates.

In terms of the local $o^{(k)}x^{(k)}y^{(k)}z^{(k)}$ system of coordinates, the Laplace transform of the heat flux intensity of rock matrix and fracture-water heat exchange can be expressed as

$$\begin{aligned}&\tilde{p}_f^k(x^{(k)},y^{(k)},0,s)=-2\lambda_r\left.\frac{\partial\tilde{T}_d(x^{(k)},y^{(k)},z^{(k)},t)}{\partial z^{(k)}}\right|_{z^{(k)}=0}\\&=-\rho_w c_w\boldsymbol{q}^{(k)}(x^{(k)},y^{(k)})\cdot\nabla_2\tilde{T}_d(x^{(k)},y^{(k)},0,s),\\&\qquad k=1-K,\end{aligned}\tag{16}$$

where T_d=T−T_0 is the variation of temperature from its initial value. The thermal elastic potential can be expressed as

$$\tilde{\Phi}(x,y,z,s)=\frac{\alpha_r(1+\nu)\rho_w c_w}{4\pi s\rho_r c_r(1-\nu)}\sum_{k=1}^{K}Q_k-\frac{\alpha_r(1+\nu)}{4\pi s\rho_r c_r(1-\nu)}Q_{\Gamma},\tag{17}$$

where

$$\begin{aligned}Q_k&=\int_{A_k}\left[\boldsymbol{q}^{(k)}(x^{(k)},y^{(k)})\cdot\nabla_2\tilde{T}_d(x^{(k)},y^{(k)},0,s)\right]\\&\cdot\left[\frac{1}{R^{(k)}}-\frac{1}{R^{(k)}}\exp\left(-\sqrt{\frac{s\rho_r c_r}{\lambda_r}}R^{(k)}\right)\right]\mathrm{d}A_k,\end{aligned}$$

$$Q_{\Gamma}=\int_{\Gamma}\tilde{p}_r(x',y',z',s)\left[\frac{1}{R_p}-\frac{1}{R_p}\exp\left(-\sqrt{\frac{s\rho_r c_r}{\lambda_r}}R_p\right)\right]\mathrm{d}\Gamma.$$

$R^{(k)}$ stands for the distance between the point $(x_r^{(k)}, y_r^{(k)}, z_r^{(k)}, 1)=(x_r, y_r, z_r, 1)\boldsymbol{C}^{(k)}\boldsymbol{F}^{(k)}$ where the thermal elastic potential is to be calculated and the point $(x^{(k)}, y^{(k)}, 0)$ on A_k for the heat flux intensity of rock matrix and fracture-water heat exchange, and R_p is the distance between the point (x_r, y_r, z_r) where the thermal elastic potential is to be calculated and the point (x', y', z') for the heat flux intensity of the line heat source.

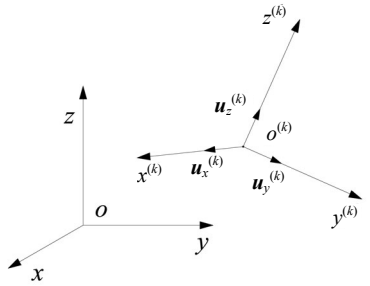

Fig. 2 Transformation of the system of coordinates. Reprinted from (Zhang and Xiang, 2014), Copyright 2014, with permission from Elsevier

Discretizing the fractures into rectangular elements, using analytical approach to calculate those elemental integrals that involve singularities, and employing the numerical approach to calculate other elemental integrals that do not contain singularities as well as the elemental integrals relevant to the distributed heat source, the numerical solution of $\tilde{\Phi}(x, y, z, s)$ and then the numerical solution of $\Phi(x, y, z, t)$ can be calculated using numerical Laplace inversion, and the temperature-gradient-induced displacement and stress can be calculated by using central differences, for example

$$u_z^T(x,y,z,t)=\frac{\partial \Phi}{\partial z}=\frac{\Phi(x,y,z+\Delta z,t)-\Phi(x,y,z-\Delta z,t)}{2\Delta z}, \tag{18}$$

$$\sigma_{zz}^T(x,y,z,t)=-2\mu\left(\frac{\partial^2\Phi}{\partial x^2}+\frac{\partial^2\Phi}{\partial y^2}\right)$$

$$=-2\mu\left[\frac{\Phi(x+\Delta x,y,z,t)-2\Phi(x,y,z,t)+\Phi(x-\Delta x,y,z,t)}{(\Delta x)^2}\right.$$

$$\left.+\frac{\Phi(x,y+\Delta y,z,t)-2\Phi(x,y,z,t)+\Phi(x,y-\Delta y,z,t)}{(\Delta y)^2}\right], \tag{19}$$

$$\sigma_{zx}^T(x,y,z,t)=2\mu\frac{\partial^2\Phi}{\partial z\partial x}=\frac{2\mu}{4\Delta z\Delta x}[\Phi(x+\Delta x,y,z+\Delta z,t)$$

$$+\Phi(x-\Delta x,y,z-\Delta z,t)-\Phi(x-\Delta x,y,z+\Delta z,t)$$

$$-\Phi(x+\Delta x,y,z-\Delta z,t)]. \tag{20}$$

The displacements and stresses in other orientations can be calculated in a similar fashion.

4 Example calculation and analysis

4.1 Heat transfer and thermal elastic model

Fig. 3 shows a heat transfer and thermal elastic model of a hypothetical radioactive waste repository involving three emplacement drifts in a saturated rock mass containing two fractures perpendicular to each other. Let the heat generated by the waste be represented by the heat sources distributed along the lines of the central axes of the three drifts, indicated by Γ_1, Γ_2, and Γ_3, respectively, and a_1, a_2, a_3, b_1, b_2, and b_3 are the starting points and ending points of the lines. Let q_h and q_v be the known no-interference, steady unit-width water fluxes in the horizontal and vertical fractures, respectively. Let L_h and L_v be the lengths of influences in the horizontal and vertical fractures, respectively, and let L_w be the width of influence for both the horizontal and vertical fractures. The calculation results will be presented along the line l_h (x=0–L_h, y=L_w/2, z=0) and the line l_v (x=180 m, y=L_w/2, z=−300–100 m), and in the plane a_r (z=7 m).

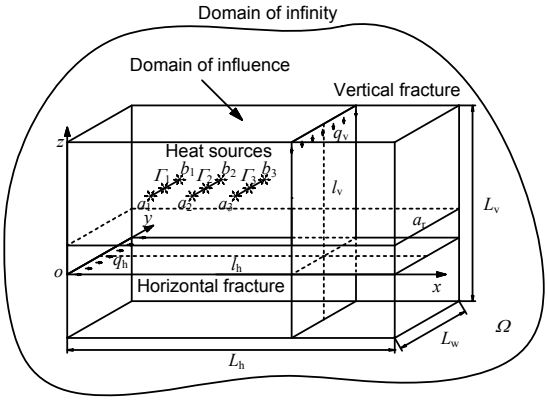

Fig. 3 Heat transfer and thermal elastic model of a hypothetical radioactive waste repository

According to Lu (2012), an exponential function may be employed to fit the temporal curve of heat source strength, given in Chijimatsu *et al.* (2005), so that the degradation of power from the canister of vitrified radioactive waste can be taken into

consideration by using a line intensity of power function in the form

$$p_r = 250\exp(-0.02t) \ \text{W/m}, \tag{21}$$

where t is the time in years after the waste is emplaced in the drifts.

To simplify the calculation, assume the physical properties of water and the rock matrix as given in Table 1, and ignore the influence of temperature variation. The parameters for the fractures and water flow are given in Table 2 (note that the apertures are given for calculating the unit-width water fluxes of the fractures). Based on trial calculations, values of the lengths and the width of influences for the fractures have been selected large enough so that both the temperature variation and the thermal effect outside this range of fractures are negligible. The locations of the heat source lines are given in Table 3.

Table 1 Physical properties of water and rock matrix

Property	Value
Rock density, ρ_r (kg/m^3)	2650
Rock specific heat, c_r (J/(kg·°C))	1000
Rock thermal conductivity, λ_r (W/(m·°C))	2.59
Rock shear modulus, μ (MPa)	1.5×10^4
Rock Poisson's ratio, ν	0.25
Rock thermal expansion coefficient, α_r (1/°C)	8.0×10^{-6}
Water density, ρ_w (kg/m^3)	1000
Water specific heat, c_w (J/(kg·°C))	4180

4.2 Distributions and evolutions of the temperature, thermal stress, and displacement

Figs. 4 and 5 show the distributions of the water temperatures of the horizontal and vertical fractures, respectively. Fig. 6 shows the distributions of the temperature of the rock matrix at the plane a_r at some selected times.

Table 2 Parameters of the fractures and water flow

Parameter	Horizontal fracture	Vertical fracture
Aperture (mm)	5	5
Water velocity (mm/s)	0.5	0.5
Position (m)	z=0	x=180
Length of influence (m)	800	400
Width of influence (m)	100	100

Table 3 Locations of the heat sources (m)

Line heat source, Γ_k	Coordinates of endpoint, a_k	Coordinates of endpoint, b_k
Γ_1	(90, 40, 10)	(90, 60, 10)
Γ_2	(130, 40, 10)	(130, 60, 10)
Γ_3	(170, 40, 10)	(170, 60, 10)

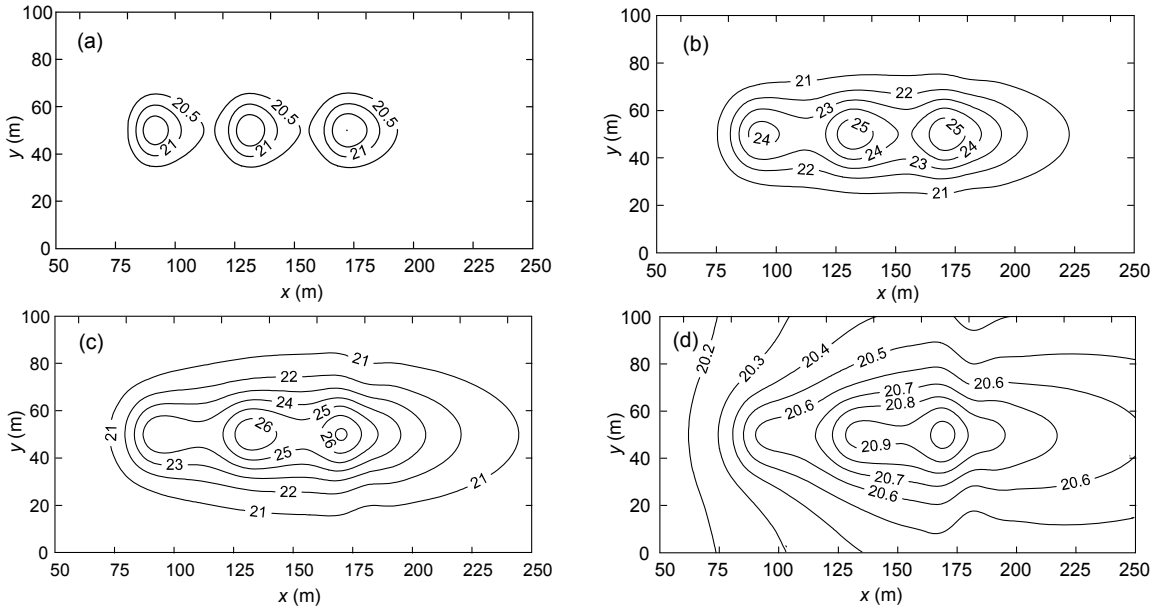

Fig. 4 Distributions of the temperature of water in the horizontal fracture at selected times (unit: °C)
(a) t=1 year; (b) t=5 year; (c) t=10 year; (d) t=150 year

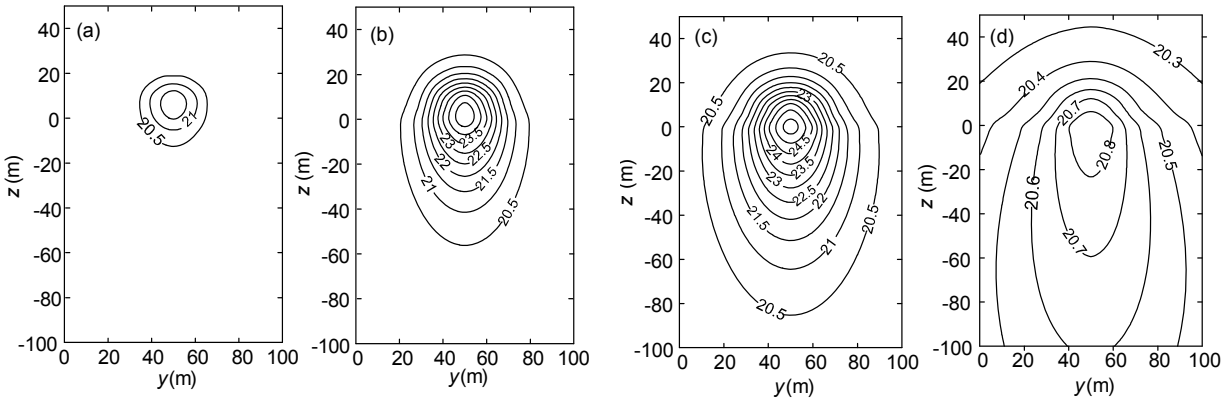

Fig. 5 Distributions of the temperature of water in the vertical fracture at selected times (unit: °C)
(a) t=1 year; (b) t=5 year; (c) t=10 year; (d) t=150 year

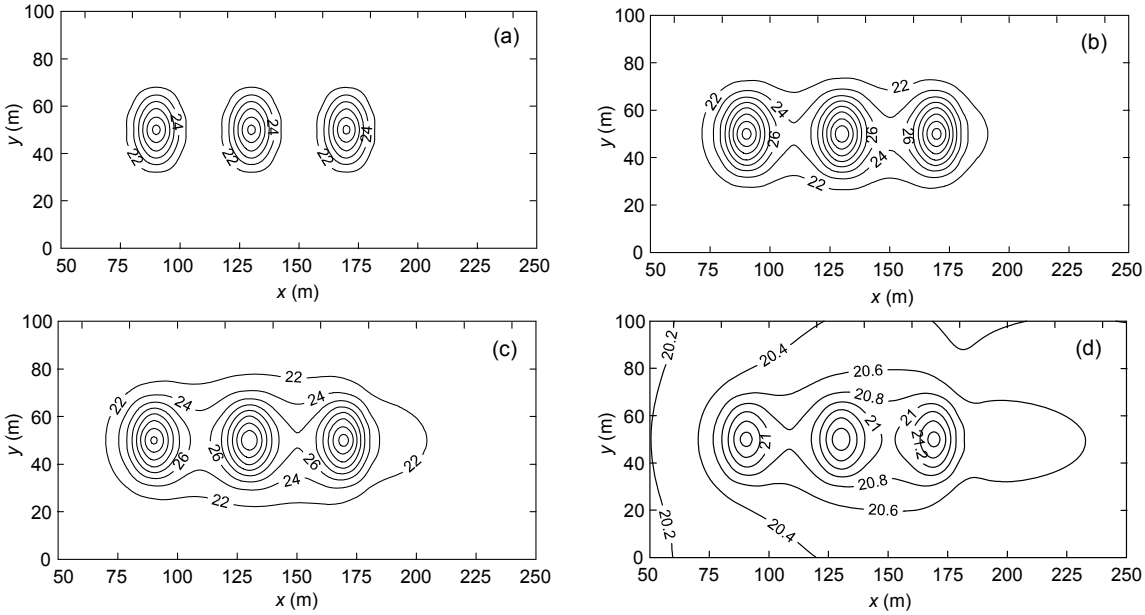

Fig. 6 Distributions of the temperature of the rock matrix at plane a_r at selected times (unit: °C)
(a) t=1 year; (b) t=5 year; (c) t=10 year; (d) t=150 year

Figs. 7 and 8 show the distributions of the temperature-gradient-induced stresses of the rock matrix normal to the intersections with the horizontal and vertical fractures, respectively, at selected times. One can see that at early time of operation of the repository, e.g., 1 year, since the range of thermal expansion of the rock is limited, the areas of the corresponding compressive stresses are relatively small, whereas there exist rather large areas of tensile stresses due to the compatibility of deformation of the areas with the areas of thermal expansion. The areas of compressive stresses increase with time, accompanied by a decrease of the areas of tensile stresses, resulting from increases of the ranges of influences of the heat sources, and at long enough time, e.g., 150 years, all areas of tensile stresses essentially disappear.

The displacements of the rock matrix at the fracture walls may cause changes in the apertures of the fractures. With this in mind, the distributions of the temperature-gradient-induced displacements of the rock matrix normal to the intersections with the horizontal and vertical fractures at selected times are

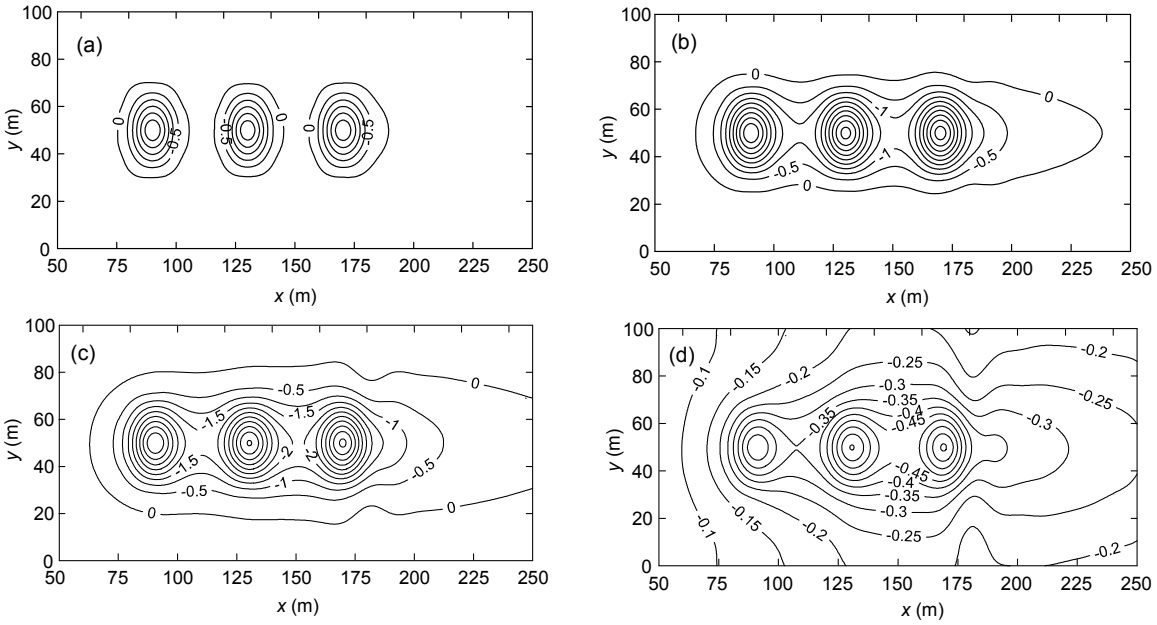

Fig. 7 Distributions of the temperature-gradient-induced stress $\sigma_{zz}{}^{T}$ of the rock matrix at the intersection with the horizontal fracture at selected times (unit: MPa): (a) t=1 year; (b) t=5 year; (c) t=10 year; (d) t=150 year

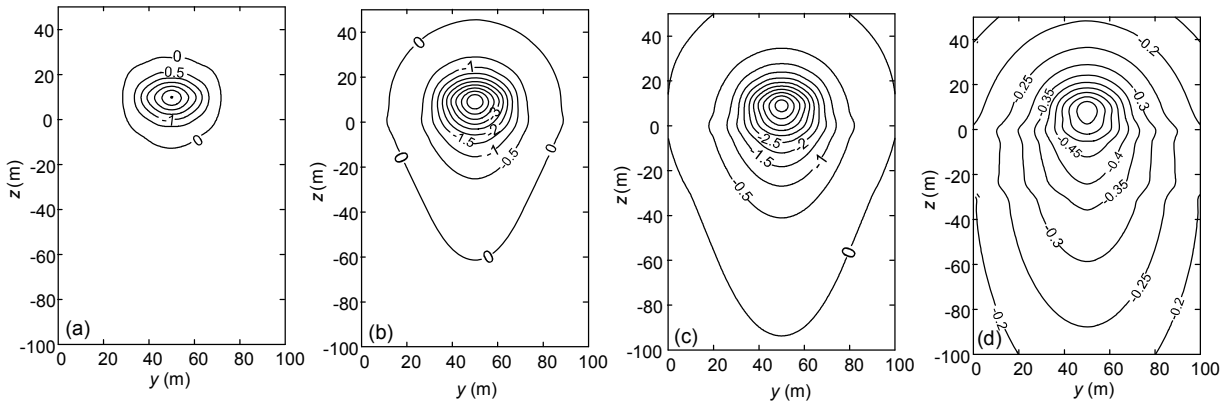

Fig. 8 Distributions of the temperature-gradient-induced stress $\sigma_{xx}{}^{T}$ of the rock matrix at the intersection with the vertical fracture at selected times (unit: MPa): (a) t=1 year; (b) t=5 year; (c) t=10 year; (d) t=150 year

shown in Figs. 9 and 10, respectively, from which one may see that the displacements are initially induced mainly by the heat sources while the influences from water-flow-facilitated heat transfer gradually get significant. It is interesting to note from Fig. 9 that, as opposed to the signs of the displacements at 1 year, 5 years, and 10 years, the displacements at the 150th year are positive, which means the rock matrix is under compression. This phenomenon may be attributed to the fact that certain amount of the thermal energy at early times has been transported out of the near-field such that the reduced intensity of the heat source at 150 years (about 12.5 W/m) can only cause a small portion of the rock matrix to expand whereas the remaining portion contracts due to compatibility of deformation.

4.3 Effects of fracture water fluxes on the temperature, thermal stress, and displacement

Figs. 11–16 show the distributions at 10 years of the water temperatures, the stresses, $\sigma_{zz}{}^{T}$ and $\sigma_{xx}{}^{T}$, and the displacements, $u_z{}^{T}$ and $u_x{}^{T}$, at the observation lines l_{h} and l_{v} of the horizontal and vertical fractures, respectively, for some selected velocities of water flow.

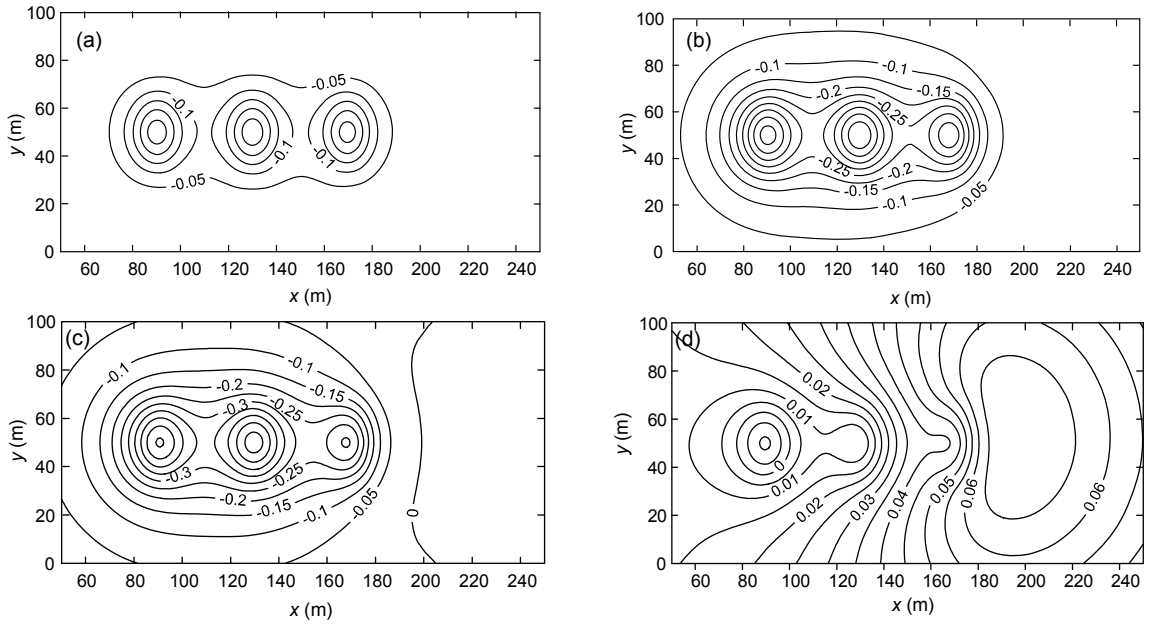

Fig. 9 Distributions of the temperature-gradient-induced displacement u_z^T of the rock matrix at the intersection with the horizontal fracture at selected times (unit: mm): (a) t=1 year; (b) t=5 year; (c) t=10 year; (d) t=150 year

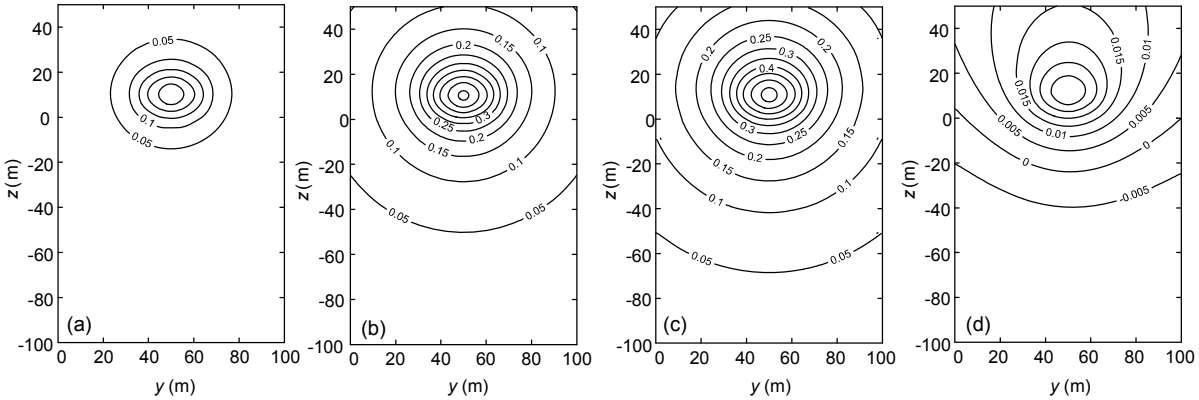

Fig. 10 Distributions of the temperature-gradient-induced displacement u_x^T of the rock matrix at the intersection with the vertical fracture at selected times (unit: mm): (a) t=1 year; (b) t=5 year; (c) t=10 year; (d) t=150 year

From Figs. 11 and 12, one may see that, among other things, the positions of the peak temperatures correspond to the orthogonal projections of the

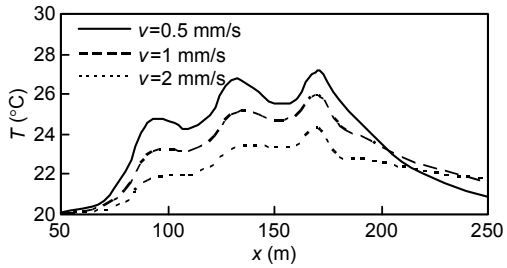

Fig. 11 Distributions of temperature along the observation line l_h for selected water velocities

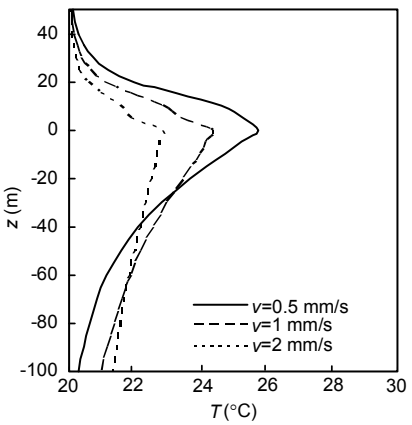

Fig. 12 Distributions of temperature along the observation line l_v for selected water velocities

positions of the heat sources on the relevant fracture planes. Specifically, for the horizontal fracture, the downstream peak temperatures are higher, due to the supply of thermal energy by the water-flow-facilitated heat transfer. Similar patterns of influences of the water velocities on the thermal stresses, $\sigma_{zz}{}^T$ and $\sigma_{xx}{}^T$, and the thermal displacements, $u_z{}^T$ and $u_x{}^T$, can be observed in Figs. 13–16, respectively.

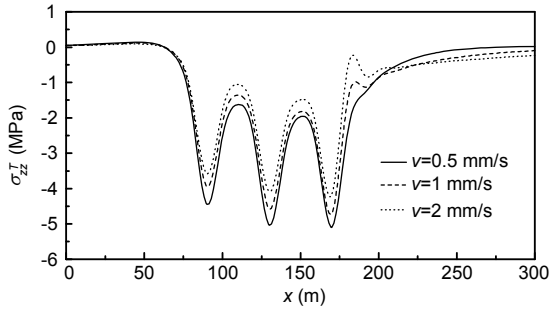

Fig. 13 Distributions of stress $\sigma_{zz}{}^T$ along the observation line l_h for selected water velocities

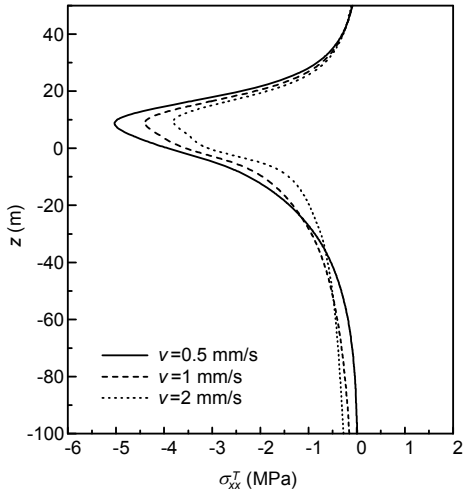

Fig. 14 Distributions of stress $\sigma_{xx}{}^T$ along the observation line l_v for selected water velocities

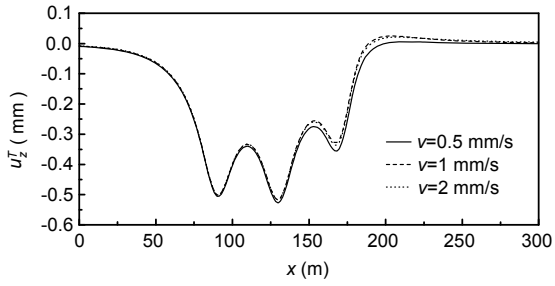

Fig. 15 Distributions of displacement $u_z{}^T$ along the observation line l_h for selected water velocities

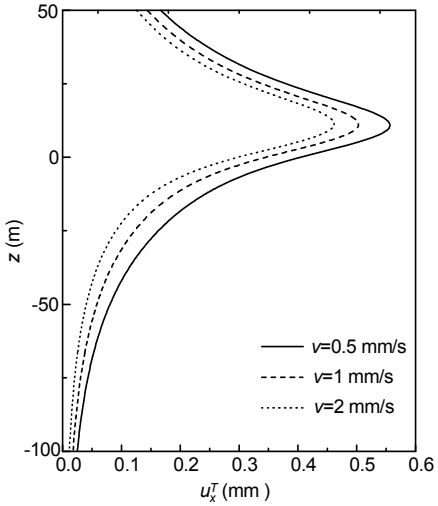

Fig. 16 Distributions of displacement $u_x{}^T$ along the observation line l_v for selected water velocities

4.4 Effects of spacing of heat sources on the temperature, thermal stress, and displacement

As shown in Table 4, we consider three different cases for the locations of the heat source lines, each with a different spacing between the heat sources. Figs. 17–22 show the distributions of the water temperatures, the stresses, $\sigma_{zz}{}^T$ and $\sigma_{xx}{}^T$, and the displacements, $u_z{}^T$ and $u_x{}^T$, at the observation lines l_h and l_v of the horizontal and vertical fractures, respectively, over 10 years for some selected heat source locations. The smaller the heat source spacing, the higher the near-field temperature, and if the heat source lines are close enough, superposition of the heating effects may cause the near-field temperature to increase significantly. Similar observations hold for the thermal stresses and displacements.

Table 4 Locations of the heat source lines (unit: m)

Heat source		Location		
		d=20	d=40	d=60
Γ_1	a_1	(130, 40, 10)	(90, 40, 10)	(50, 40, 10)
	b_1	(130, 60, 10)	(90, 60, 10)	(50, 60, 10)
Γ_2	a_2	(150, 40, 10)	(130, 40, 10)	(110, 40, 10)
	b_2	(150, 60, 10)	(130, 60, 10)	(110, 60, 10)
Γ_3	a_3	(170, 40, 10)	(170, 40, 10)	(170, 40, 10)
	b_3	(170, 60, 10)	(170, 60, 10)	(170, 60, 10)

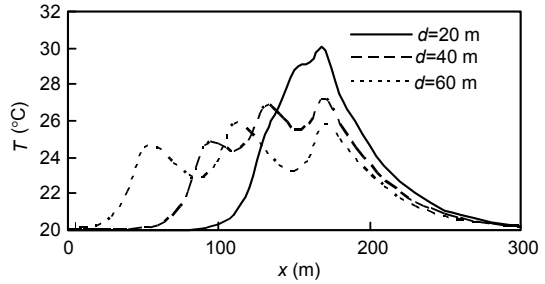

Fig. 17 Distributions of temperature along the observation line l_h for selected heat source locations

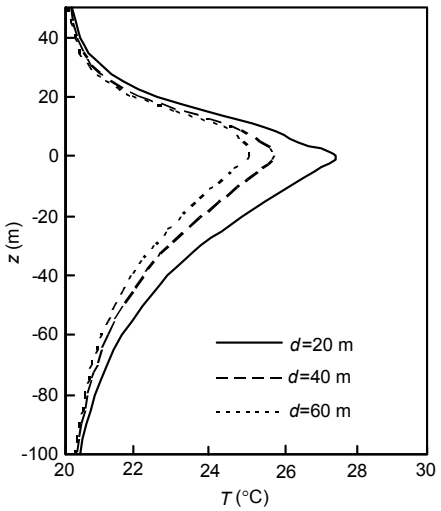

Fig. 18 Distributions of temperature along the observation line l_v for selected heat source locations

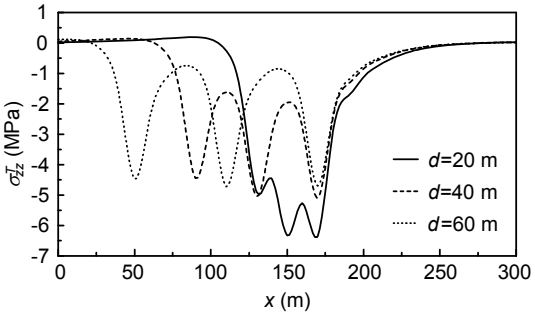

Fig. 19 Distributions of stress σ_{zz}^T along the observation line l_h for selected heat source locations

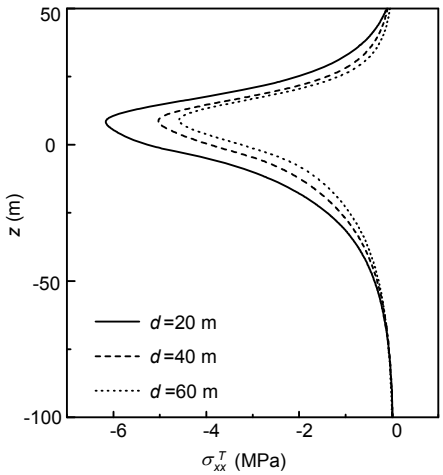

Fig. 20 Distributions of stress σ_{xx}^T along the observation line l_v for selected heat source locations

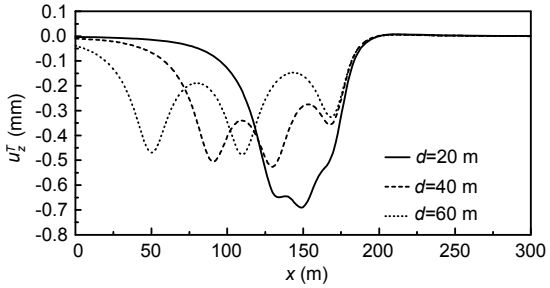

Fig. 21 Distributions of displacement u_z^T along the observation line l_h for selected heat source locations

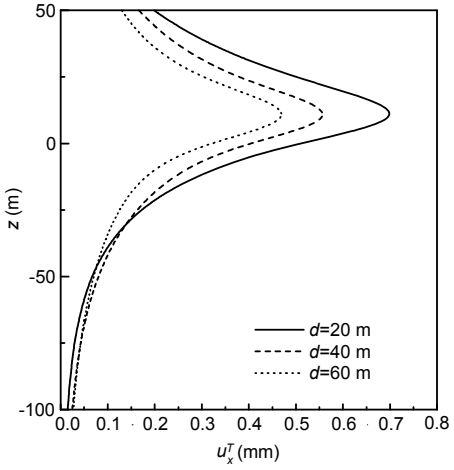

Fig. 22 Distributions of displacement u_x^T along the observation line l_v for selected heat source locations

5 Conclusions

A semi-analytical method has been developed for calculating the displacement and stress induced by heat transfer in sparsely fractured granitic rocks with saturated water flow and distributed heat sources. With special regard to the near-field environment of deep geological repositories of vitrified high-level radioactive wastes, the method was applied to examine the characteristics of the temperature-gradient-induced displacement and stress of a hypothetical problem that involved water flow in two intersecting

fractures and three line heat sources. One possible application of the proposed method could be in the prediction of thermally induced displacements and stresses in saturated sparsely fractured rocks for assessing, in conjunction with other means of simulations, the designs of deep repositories of high-level radioactive wastes.

Based on the calculations, the following phenomena may be observed: (1) In early time of operation of the repository, the region of rock under thermal expansion and compressive stress is limited, whereas due to compatibility of deformation, tensile stress occurs in nearby region; (2) After certain amount of the thermal energy at early times has been transported out of the near-field, and as the intensities of the heat sources get smaller, only a small portion of the rock matrix expands whereas the remaining portion contracts; (3) The positions of the peak temperatures of water in the fractures correspond to the orthogonal projections of the positions of the heat sources on the relevant fracture planes, the downstream peak temperatures may be higher due to the supply of thermal energy by water-flow-facilitated heat transfer, and patterns of influences of the water velocities on the thermal stress and displacement are similar; (4) A smaller spacing between the heat sources results in a higher near-field temperature, and sufficiently close heat sources would cause superposition of the heating effects and high near-field temperature.

One limitation of the semi-analytical calculations presented here is that the effect of fracture aperture change has not been considered. Further study is needed to incorporate such effect in the analysis.

References

Carslaw, H.S., Jaeger, J.C., 1959. Conduction of Heat in Solids. Oxford University Press, New York.

Chijimatsu, M., Nguyen, T.S., Jing, L., *et al.*, 2005. Numerical study of the THM effects on the near-field safety of a hypothetical nuclear waste repository—BMT1 of the DECOVALEX III project. Part 1: conceptualization and characterization of the problems and summary of results. *International Journal of Rock Mechanics and Mining Science*, **42**(5-6):720-730. [doi:10.1016/j.ijrmms.2005.03.010]

Ghassemi, A., Zhang, Q., 2006. Porothermoelastic analysis of the response of a stationary crack using the displacement discontinuity method. *Journal of Engineering Mechanics*, **132**(1):26-33. [doi:10.1061/(ASCE)0733-9399(2006)132:1(26)]

Gutierrez, M., Makurat, A., 1997. Coupled HTM modelling of cold water injection in fractured hydrocarbon reservoirs. *International Journal of Rock Mechanics and Mining Sciences*, **34**(3-4):111-113. [doi:10.1016/S0148-9062(97)00033-8]

Lu, W., 2012. Model Experiment and Calculation Theory of Water Flow and Heat Transfer in Fractured Rocks. PhD Thesis, Beijing Jiaotong University, China (in Chinese).

Onofrei, C., Gray, M., 1996. Modelling hydro-thermo-mechanical behaviour of engineered clay—barriers validation phase. *Engineering Geology*, **41**(1-4):301-318. [doi:10.1016/0013-7952(95)00052-6]

Rutqvist, J., Börgesson, L., Chijimatsu, M., *et al*., 2001. Coupled thermo-hydro-mechanical analysis of a heater test in fractured rock and bentonite at Kamaishi Mine—comparison of field results to predictions of four finite element codes. *International Journal of Rock Mechanics and Mining Sciences*, **38**(1):129-142. [doi:10.1016/S1365-1609(00)00069-1]

Tortike, W.S., Ali, S.M.F., 1991. Prediction of oil sand failure due to steam-induced stresses. *Journal of Canadian Petroleum Technology*, **30**(1):87-96. [doi:10.2118/91-01-08]

Tortike, W.S., Ali, S.M.F., 1993. Reservoir simulation integrated with geomechanics. *Journal of Canadian Petroleum Technology*, **32**(5):28-37. [doi:10.2118/93-05-02]

Wang, H., 1989. Fundamental Theory of Thermo-elasticity. Tsinghua University Press, Beijing (in Chinese).

Zhang, Y., Xiang, Y., 2014. A semi-analytical modeling approach for three-dimensional heat transfer in sparsely fractured rocks with water flow and distributed heat source. *International Journal for Numerical and Analytical Methods in Geomechanics*, **38**(11):1149-1171. [doi:10.1002/nag.2252]

Zhang, Y., Xiang, Y., 2015. A semi-analytical approach for calculation of displacement and stress in the processes of 3-D water flow and heat transfer in saturated sparsely fractured rock mass. *Rock and Soil Mechanics*, in press (in Chinese).

Zhou, X.X., Ghassemi, A., Cheng, A.H.D., 2009. A three-dimensional integral equation model for calculating poro- and thermoelastic stresses induced by cold water injection into a geothermal reservoir. *International Journal for Numerical and Analytical Methods in Geomechanics*, **33**(14):1613-1640. [doi:10.1002/nag.780]

中文概要

题　目：稀疏裂隙岩体水流传热过程中热应力及位移的半解析计算方法和应用

目　的：探索核废料地质处置库近场岩体在热源（核素衰变产生热量）和裂隙水流动影响下的应力和变形规律，为处置库的安全评估提供理论基础。

创新点：针对包含内热源和饱和裂隙水流动的岩体，提出一种稀疏裂隙岩体水流传热过程中热应力及位

移的半解析计算方法，并将该方法应用于核废物处置库近场裂隙岩体温度、热应力和位移的分布特征分析。

方　法：首先根据热弹性位移势法建立拉普拉斯变换域内的基本积分方程，然后将裂隙离散化，利用数值积分方法计算不含奇点的裂隙单元积分，采用解析法计算包含奇点的单元积分，再根据拉普拉斯数值逆变换将热弹性位移势转换到时间域中，最后利用中心差分法计算热应力和位移。

结　论：1. 在处置库运营早期，岩石受分布热源影响而产生热膨胀区域的范围（即受压区域）较为有限；2. 核素在经过长期的衰变过程后，热流强度大幅降低，使得处置库近场岩石中仅有热源附近的极小部分岩石为受压区域；3. 裂隙水的流动传热作用使得处置库下游的温度峰值更高，且裂隙水流速越大，流动传热作用越明显，裂隙水流速对热应力和位移的影响与温度类似；4. 过小的热源间距会使不同热源间传热作用叠加，从而导致处置库近场的温度、热应力和位移峰值急剧增大。

关键词：稀疏裂隙岩体；裂隙水流；热传导；热弹性位移势；热应力